ACS APPLIED MATERIALS & INTERFACES

Research Article

www.acsami.org

Polyaniline–Carbon Nanofiber Composite by a Chemical Grafting Approach and Its Supercapacitor Application

Moumita Kotal,[†] Awalendra K. Thakur,[‡] and Anil K. Bhowmick*,[†]

[†]Department of Chemistry and [‡]Department of Physics,Indian Institute of Technology, Patna 800013, India

Supporting Information

ABSTRACT: Unlike conventional routes by van der Waals forces, a facile and novel approach using covalent bonding is established in the present work to synthesize polyaniline (PANI)-grafted carbon nanofiber (CNF) composites as promising supercapacitors. For this purpose, toluenediisocyanate was initially functionalized to carboxylated CNF via amidation followed by reaction with excess aniline to form a urea derivative and residual aniline, which was subsequently polymerized and grafted with a urea derivative. Amidation of CNF (TCNF) and, consequently, the grafting of PANI on TCNF were verified by IR, Raman, ^{1}H NMR, X-ray photoelectron, and UV–visible spectroscopic methods, X-ray diffraction, and thermogravimetric analysis. Morphological analysis revealed uniform distribution of PANI on the surface of TCNF, indicating strong interaction between them. Electrochemical tests of the composite containing 6 wt % TCNF demonstrated efficient capacitance of ~557 F g^{-1} with a capacity retention of 86% of its initial capacitance even after 2000 charge–discharge cycles at a current density of 0.3 A g^{-1}, suggesting its superiority compared to the materials formed by van der Waals forces. The remarkably enhanced electrochemical performance showed the importance of the phenyl-substituted amide linkage in the development of a π-conjugated structure, which facilitated charge transfer and, consequently, made it attractive for efficient supercapacitors.

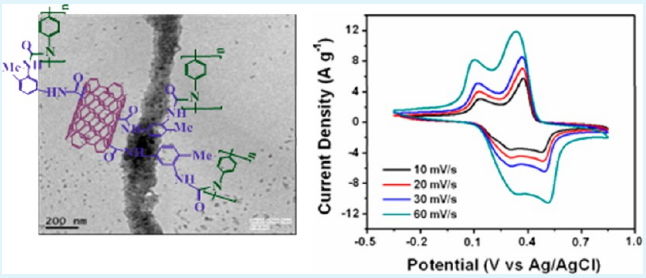

KEYWORDS: *carbon nanofiber, polyaniline, composites, chemical grafting, supercapacitor, electrochemical properties*

INTRODUCTION

In the wake of depleting fossil fuel reserve and increasing awareness for pollution control, industry and research centers around the world are searching for viable alternatives to the development of renewable energy production that can compete with all available technologies.[1] In this quest, supercapacitors, known as electrochemical capacitors or ultracapacitors, represent an attractive substitute for portable electronics and automotive applications in view of their higher power density, reversibility, and longer cycle life compared to secondary batteries.[2−6] In fact, electrochemical capacitors serve the purpose of rising demand of transferable power systems and hybrid electric vehicles, which involve high power delivery in a short time. Formations of electrical double layer (EDL) capacitance and pseudocapacitance are the two basic mechanisms for energy storage in supercapacitors. The former one is a non-Faradic process because it stores charges electrostatically via reversible ion absorption at the electrode–electrolyte interface,[7] while in the later type, Faradic charge transfer takes place at the electrode materials.[8,9] Carbonaceous materials, for example, carbon nanofibers (CNFs), carbon nanotubes (CNTs), and graphene, are generally used as symmetric electrodes for EDL capacitors because of their large surface area, porous structures, good thermal and chemical stability, high electrical conductivity and mechanical properties, and long cycling stability, although these microstructures have limited the value of the capacitance.[2,10] On the contrary, metal oxides (e.g., RuO_2, MnO_2, and Mn_3O_4)[11−13] and lightweight conducting polymers [e.g., polyaniline (PANI), polypyrrole, and polythiophene][14,15] are considered suitable for pseudocapacitors with relatively high capacitance. However, they exhibit inferior cyclability due to structural deterioration of the electrodes originating from the generation of positively charged sites on the polymer chains during the charge–discharge process, which, in turn, lowers the electrode's electrical conductivity.[16−18] Therefore, composites based on the appropriate stoichiometric combination of carbonaceous materials and conducting polymers have been proven to be a potential breakthrough for a new generation of efficient supercapacitors.[17−19] Hence, the research on the development of high-performance supercapacitors originating from the synergistic combination of outstanding conducting properties of carbonaceous materials and high pseudocapacitance of conducting polymers is an ongoing interest in nanotechnology.[14−23] Although supercapacitors of transition-metal oxides and conducting polymers have widely been reported,[24] work on carbon-based materials with conducting polymers as promising supercapacitors is in its nascent state.[14−23]

Received: April 17, 2013
Accepted: August 5, 2013
Published: August 5, 2013

Scheme 1. Schematic Diagram for the Preparation of a PANI-*g*-TCNF Composite by Functionalizing XCNF with TDI through Amidation Followed by Reaction with Excess Aniline To Form a Urea Derivative and Residual Aniline, Which Was Subsequently Polymerized and Grafted with a Urea Derivative

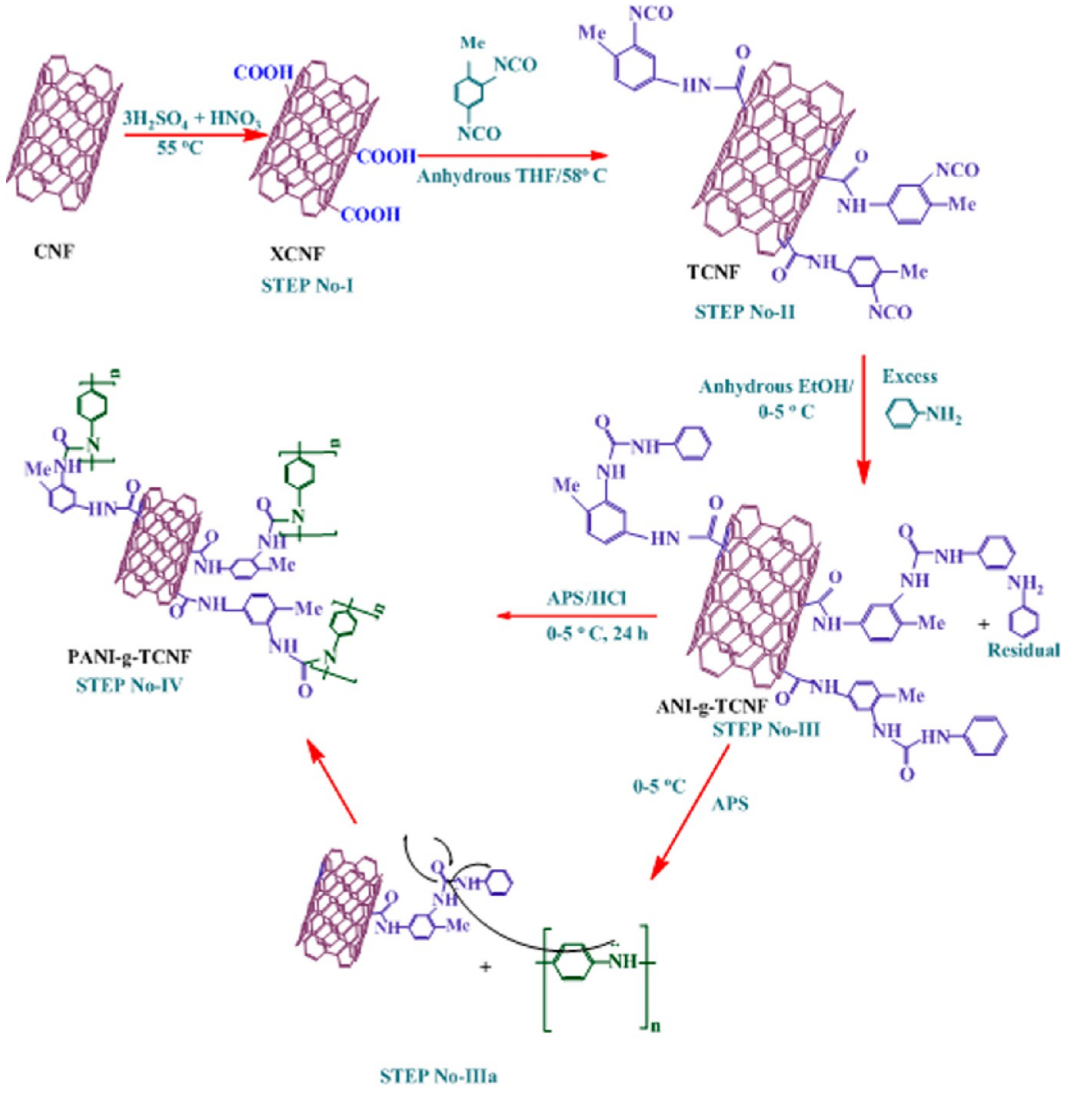

Nonetheless, some of the conducting polymers have inferior conductivity and rigidity, which limit their applicability in devices.[25] Among different conducting polymers, PANI has shown great potential for supercapacitor applications owing to its low cost of raw materials, excellent environmental stability, ease of synthesis, biocompatibility, fast redox rate, high reversible pseudocapacitance, relatively high level of electrical conductivity, and unusual doping−dedoping chemistry.[26,27] Furthermore, PANI has frequently been used to prepare composites with carbon nanomaterials for supercapacitors and sensors because their combination can not only improve the PANI conductivity but also relieve the aggregation of carbon-based materials.[28−32] However, among the aforementioned carbon-based materials, CNTs are still very expensive and the preparation of graphene is complex.[32] Therefore, alternative carbonaceous materials like readily available CNFs have recently attracted great interest in diverse application areas because of their unique one-dimensional nanostructure, excellent thermal, mechanical, and electrical properties, and potentially low manufacturing cost.[32−36] Besides these, CNFs have high surface area, which can expose entirely either basal graphite planes or edge planes. Therefore, interest in the development of electrodes, based on composites of CNF and PANI as supercapacitors, has been growing recently.[36] Jang et al.[36] prepared PANI-coated CNF with a specific capacitance of 264 F g^{-1} using a vapor deposition polymerization technique. However, pristine CNFs are not easily dispersed in liquid media and thereby have poor compatibility with PANI. As a result, their inevitable aggregation limits their application as supercapacitor materials with unsatisfactory capacitance, and to date, a scalable method has not yet been explored. In order to resolve this difficulty, surface-modified CNFs with different functional groups have to be developed for preparing supercapacitors.[37] Moreover, functionalized CNFs exhibit large surface-to-volume ratios, better mechanical properties, and a wide electrochemical window comparable to their ordinary porous and activated carbon atoms. Therefore, these are attractive materials for supercapacitors. In this regard, carboxyl-functionalized CNF-based materials with tunable oxygen functionalities on their basal planes facilitate their hybridization with PANI.

However, van der Waals forces of interaction between carboxyl-functionalized CNF and PANI render poor compat-

dx.doi.org/10.1021/am4014049 | ACS Appl. Mater. Interfaces 2013, 5, 8374−8386

ibility as well as poor capacitance like previously reported graphene−PANI or CNTs−PANI composites.[36−39] On the other hand, covalent interactions, stronger than van der Waals forces, can make them more intimate, resulting in decreased interfacial resistance, enhanced ionic transport, and thereby accelerating charge transfer, improving cyclability and capacitance performances.[40,41] Therefore, the "grafting to" approach is to be carried out for grafting PANI with functionalized CNFs with an aim to increase the electrochemical capacitance as well as lower the fabrication cost.

In this article, a novel route to develop a CNF−PANI composite by grafting PANI onto isocyanate-functionalized CNF via an amide group in a three-step process is established for the first time and is shown in Scheme 1. Our strategy involves the covalent functionalization of toluenediisocyanate (TDI) to carboxylated CNF (XCNF) to give amide-functionalized CNF (TCNF; Step No-II), which is subsequently reacted with excess aniline to give a urea derivative on its surface (ANI-*g*-TCNF) and residual aniline (Step No-III), followed by in situ chemical oxidative polymerization of the aniline monomer in the presence of ammonium peroxydisulfate (Step No-IIIa), which again reacts with a urea derivative to form finally a PANI-*g*-TCNF composite (Step No-IV). The cost-effective TDI is selected as the modifying agent because of its high reactivity with the carboxyl group of XCNF without using any catalyst as well as its further functionalization to give dense PANI on the TCNF surface. The phenyl-substituted amide linkage plays an important role in connecting PANI and CNF, leading to the development of a π-conjugated system. Such a type of highly conducting network may facilitate effective transfer of the Faradic charge through the CNF network. The charges may be prohibited from accumulating, thus retarding degradation of the structural conformation of PANI with a repetitive charge−discharge process. As a result, the rate capability of a TCNF−PANI composite in terms of fast charge−discharge kinetics and rapid ion diffusion is expected to be improved by facilitating charge transfer between them and decreasing the overall resistance. The development of microstructures and their properties were analyzed accordingly using different techniques. Moreover, the electrochemical behaviors of the prepared electrode materials were studied by cyclic voltammetry (CV), electrochemical impedance spectroscopy (EIS), and galvanostatic charge−discharge (GCD) measurements. In order to understand the effect of the covalent functionalization technique, a PANI−XCNF-based composite was also synthesized and its electrochemical performance was studied for comparison.

EXPERIMENTAL SECTION

Materials. CNF (as-grown-grade PR-24-PS-LD Pyrograf-III) was procured from Pyrograf Products Inc. (Cedarville, OH). Aniline (stored in a refrigerator), ammonium peroxydisulfate (APS), toluenediisocyanate (TDI), anhydrous tetrahydrofuran (THF), and ethanol were procured from Sigma-Aldrich (St. Louis, MO). HNO_3, H_2SO_4, and HCl were obtained from Merck (Whitehouse Station, NJ). Prior to use, aniline was distilled under reduced pressure, and all of the chemicals were used as received.

Synthesis of TDI-Modified CNFs (TCNFs). At first, XCNF were prepared according to the reported method.[42−44] A total of 50 mg of CNFs was sonicated in 200 mL of a mixture of concentrated H_2SO_4 (98 vol %) and HNO_3 (70 vol %) in a volume ratio of 3:1 for 5 h at 55 °C, followed by washing with deionized water by several centrifugations, and filtering with 0.22-μm poly(tetrafluoroethylene) (PTFE) filter paper. The resulting nanofibers were dried at 100 °C under vacuum overnight. The −COOH group content of XCNF was determined by titrating with a NaOH aqueous solution.[45] After that, amidation of the XCNFs was carried out by dispersing 0.05 g of XCNF in 30 mL of anhydrous THF through sonication, followed by refluxing with 130 μL (0.901 mmol) of TDI under a N_2 atmosphere with stirring for 24 h. The as-synthesized isocyanate-functionalized CNFs were filtered through 0.22-μm PTFE filter paper and washed with anhydrous THF to completely remove the residuals. After vacuum drying at 50 °C for 12 h, TCNFs were obtained.

Synthesis of PANI-Grafted Isocyanate-Functionalized CNF (PANI-*g*-TCNF) and PANI-Carboxylated CNF (PANI−XCNF) Composites. PANI-*g*-TCNF composites were synthesized by in situ polymerization of an aniline monomer in the presence of TCNF. The weight ratio of aniline to TCNF was 100:2.13, 100:4.25, and 100:6.38. Initially, TCNF was dispersed in anhydrous ethanol (1, 2, and 3 mg mL^{-1}, 30 mL) by ultrasonication for 10 min followed by the addition of 1.38 mL of aniline under stirring for 2 h under a N_2 atmosphere at ice temperature. After that, a small amount of the solution was taken from the reaction mixture in order to understand whether a urea derivative formed or not. Then, a freshly prepared solution of 3.422 g of APS in 10 mL of HCl (1 mol L^{-1}) was dropwise added into the reaction system under ice temperature. After a few minutes, the dark suspension changed to green, demonstrating the initiation of polymerization of aniline, which was continued for 24 h under an ice bath. The obtained deep-green products were filtered after washing with HCl to eliminate any unreacted monomer. Subsequently, these materials were repeatedly washed with deionized water, acetone, and ethanol in sequence until the filtrate was colorless and finally freeze-dried under reduced pressure for 24 h to obtain PANI-*g*-TCNF composites of varying TCNF. For comparison, PANI was also synthesized without using TCNF by the same procedure. PANI-*g*-TCNF composites having about 2, 4, and 6 wt % TCNF are symbolized as PANI-*g*-2TCNF, PANI-*g*-4TCNF, and PANI-*g*-6TCNF composites, respectively. In order to explore the effect of covalent functionalization of TCNF with PANI, 6 wt % of a XCNF-based PANI composite was also synthesized using the same procedure by taking the 100:6 weight ratio of aniline to XCNF and denoted as PANI−6XCNF.

Characterizations of Pristine CNF and Synthesized Materials. Fourier transform infrared (FTIR) spectra (Perkin-Elmer spectrum 400) were recorded using pressed KBr pellets over the wavenumber range of 450−4000 cm^{-1} to determine the modification of CNF and the grafting of PANI on TCNF in the composites. Raman spectra were collected on a STR500 series (Seki Technotron) with a 514-nm laser source. The incident laser power was restricted to be less than 4 mW so as to prevent the damage of the samples induced by laser. ^1H NMR spectra were recorded on a Bruker 400 MHz spectrometer at room temperature, and δ values are relative to Me_4Si (TMS). For this purpose, a PANI-*g*-TCNF composite was dissolved in deuterated dimethyl sulfoxide (DMSO-d_6) upon heating at around 40 °C. To confirm that changes had taken place due to modification of CNF by TDI as well as grafting of PANI on TCNF, X-ray photoelectron spectroscopy (XPS) measurements were made on a VG Scientific ESCA Lab II spectrometer using electrostatic lens mode with a pass energy of 180 eV. Mg Kα radiation was used as the excitation source. UV−visible spectra were recorded on a Shimadzu UV-2550 spectrometer. X-ray diffraction (XRD) patterns were recorded in the 2θ range from 5 to 80° using a Rigaku TT RAX 3 with Cu Kα radiation (35 kV, 20 mA, λ = 0.154 nm) at a scan rate of 2° min^{-1}. The microstructures of the pristine and modified CNFs along with their composites with PANI were studied by field-emission scanning electron microscopy (FESEM; Hitachi S4800). Tapping-mode atomic force microscopy (AFM) was performed on an Agilent 5500 AFM instrument with a silicon tip under ambient conditions, and images were acquired using *Pico view 1.8* software. The distribution of PANI on a modified CNF surface was studied using transmission electron microscopy (TEM; Philips-Oxford CM 12) at an acceleration voltage of 200 kV. Thermogravimetric analysis (TGA) was carried out on a TA Instruments SDT Q 600 model at a heating rate of 10 °C

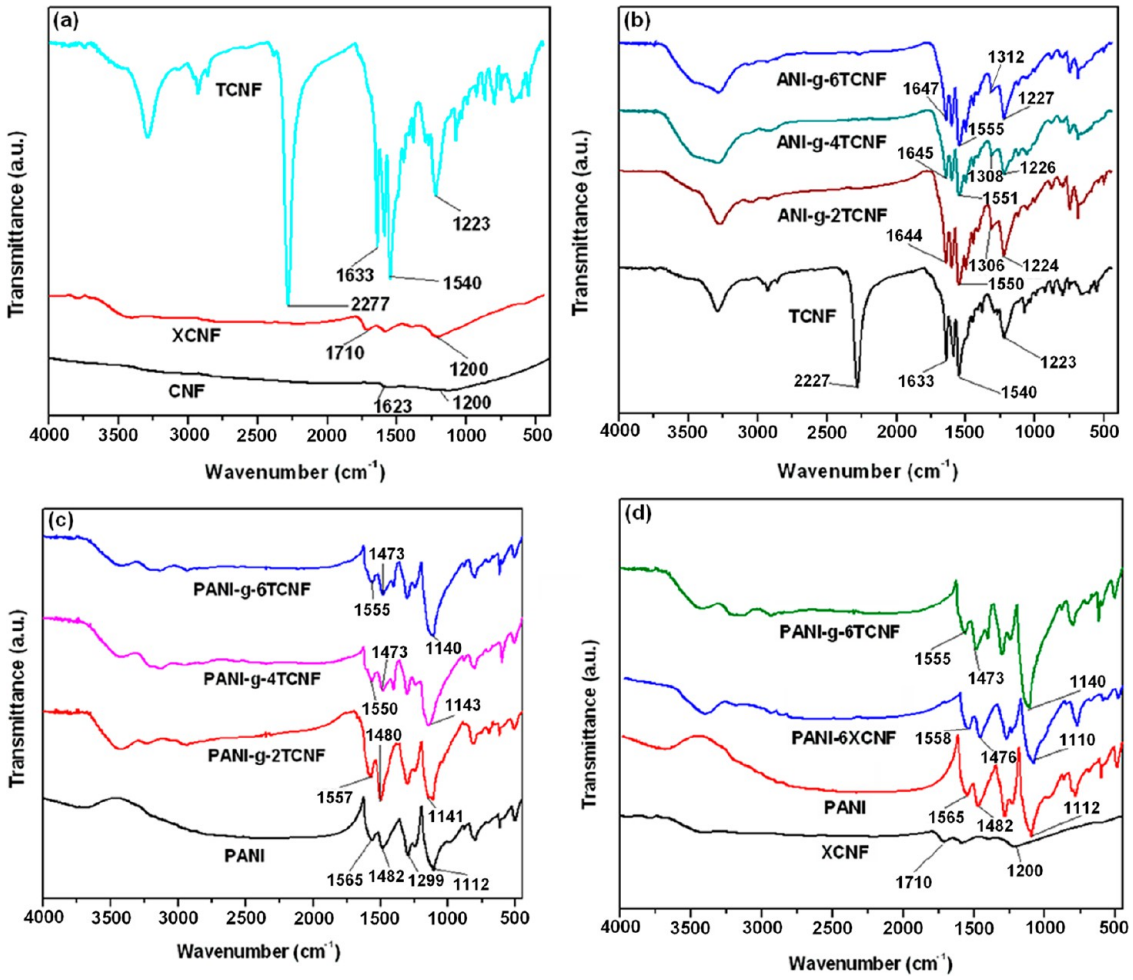

Figure 1. FTIR spectra of (a) CNF, XCNF, and TCNF, (b) TCNF along with the products formed after reaction with an aniline monomer with varying weight percentages of TCNF (2, 4, and 6 wt %), (c) PANI and PANI-*g*-TCNF composites with varying TCNF (2, 4, and 6 wt %), and (d) XCNF, PANI, and composites of PANI with 6 wt % XCNF and 6 wt % TCNF.

min^{-1} over the temperature range of 30−800 °C under a N_2 atmosphere.

Electrochemical Properties. The electrochemical measurements, namely, CV, EIS, and GCD, were performed on a CH760D electrochemical workstation (CH Instruments, Inc., Austin, TX) using a conventional three-electrode cell. The composites along with CNF, TCNF, and PANI were individually loaded on a glassy carbon electrode (GCE) acting as the working electrode, Ag/AgCl as the reference electrode, a platinum wire as the counter electrode, and 1 M aqueous H_2SO_4 solution as the electrolyte. An aqueous H_2SO_4 solution electrolyte was used considering its low cost and ease of fabrication in ambient conditions following earlier publications.[29,32] Before using GCE (3 mm diameter), it was polished with finer emery paper, cleaned in an ultrasonic bath by deionized water, and dried in air. For loading of composites on GCE, separately CNF, TCNF, PANI, and a PANI-*g*-TCNF composite were dispersed/dissolved in *N*-methylpyrrolidinone with 200 μL of a Nafion solution by ultrasonication for 6 min to make a uniform solution, of which 50 μL was deposited on GCE followed by drying at 60 °C for 5 min. The applied potential range for CV and GCD was maintained in the limits from −0.35 to 0.85 V because the decomposition voltage of 1 M aqueous H_2SO_4 electrolyte is 1.4 V in kinetic terms.[8] The sweep frequency for EIS was 10^5−0.001 Hz with an alternating-current (ac) amplitude of 5 mV against the open-circuit potential. The specific capacitance (C_s) of CNF, TCNF, PANI, and a PANI composite of XCNF and varying loading of TCNF was calculated from their charge−discharge curves using the following equation:[8]

$$C_s = \frac{I\Delta t}{m\Delta V} \quad (1)$$

where I is the discharge current, Δt is the time required for discharging the capacitor during the voltage drop of ΔV upon discharging (excluding the IR drop), and m is the mass of the active material deposited on a GCE. The amount of electroactive materials deposited on a GCE was 1.47×10^{-3} g for PANI, 1.46×10^{-3} g for CNF, 1.50×10^{-3} g for TCNF, 1.50×10^{-3} g for PANI−6XCNF, 1.47×10^{-3} g for PANI-*g*-2TCNF, 1.48×10^{-3} g for PANI-*g*-4TCNF, and 1.50×10^{-3} g for PANI-*g*-6TCNF.

RESULTS AND DISCUSSION

FTIR was used to elucidate the carboxylation of CNF, the modification on carboxylated CNF (TCNF) by TDI, and finally the grafting of PANI with TCNF in this study. As shown in Figure 1a, the absorption band at 1623 cm^{-1} and a broad band at 1296−1009 cm^{-1} are assigned to C═C stretching originating from the inherent structure of CNFs and C−O stretching vibration, respectively.[46] XCNF shows strong absorption bands at 1710 and 1200 cm^{-1} corresponding to −C═O stretching of −COOH and the −C−O stretching frequency of C−OH/C−O−C groups, respectively, which satisfy the carboxylation of CNF (shown in Scheme 1, Step No-I). In TCNF, there is a peak at around 2277 cm^{-1}, characteristic for asymmetric stretching of the −NCO groups, suggesting

dx.doi.org/10.1021/am4014049 | ACS Appl. Mater. Interfaces 2013, 5, 8374−8386

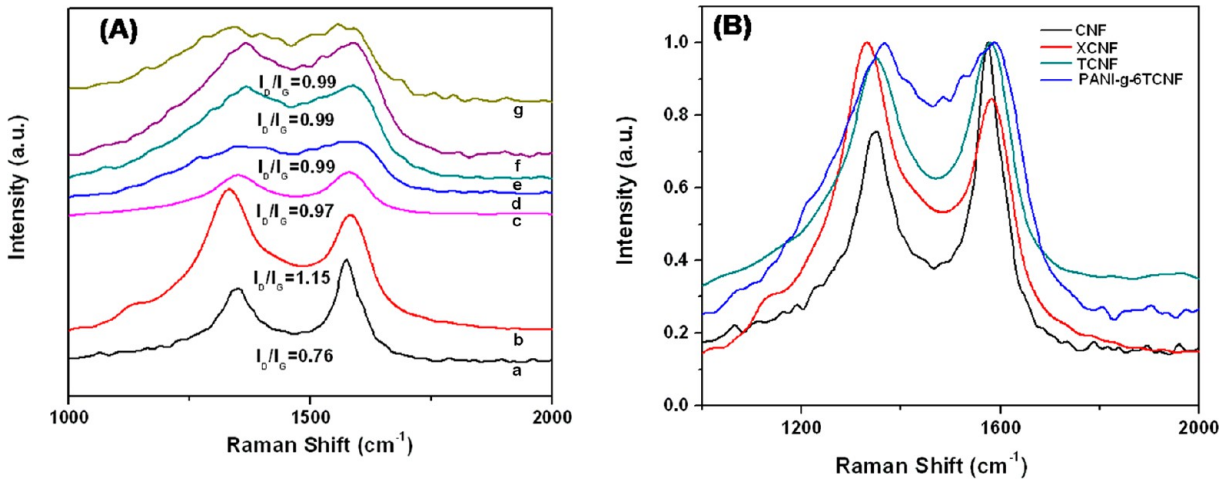

Figure 2. (A) Raman spectra of (a) CNF, (b) XCNF, (c) TCNF, and PANI-*g*-TCNF composites with (d) 2, (e) 4, and (f) 6 wt % TCNF and (g) PANI and (B) normalized Raman spectra of CNF, XCNF, TCNF, and a PANI-*g*-6TCNF composite by taking the maximum value of the G band.

successful grafting of TDI with XCNF, as shown in Scheme 1, Step No-II. The stretching frequencies of amide I (C═O of −CONH) at 1633 cm^{-1} and amide II (−NH bending vibration) at 1540 cm^{-1} further support amide bond formation between the −NCO group of TDI and the −COOH group of XCNF.[47] A calibration curve for determining the level of grafting by FTIR analysis was established using a series of quantitative amounts of TDI by plotting absorbance of the −NCO stretching frequency against the millimolar amount of TDI (as shown in Figure S1 in the Supporting Information, SI). From a linear regression plot of the calibration curve of TDI, the percentage of grafting was calculated using the absorbance corresponding to the grafted product. Therefore, the millimolar amount of excess isocyanate in TCNF was calculated, and thereby the percentage of grafting was evaluated to be 33.69%.

FTIR spectra of TCNF along with the products formed after reaction with an aniline monomer are shown in Figure 1b in order to understand whether a urea derivative formed or not. As expected, the characteristic −NCO peak disappears, indicating successful grafting of free −NCO of TCNF with aniline in all of the composites having different contents of TCNF. Also, in all of these three cases, characteristic urea bands are observed at 1644, 1645, and 1647 cm^{-1} (amide I), 1550, 1551, and 1556 cm^{-1} (amide II), and 1306, 1308, and 1312 cm^{-1} (asymmetric N−C−N stretch), providing support for the formation of a urea bond by the reaction of a terminal isocyanate group of TCNF with aniline, as shown in Scheme 1, Step No-III.[48]

After polymerization of aniline on TCNF in the presence of APS, FTIR spectra were also collected. This is shown in Figure 1c along with that of PANI for comparison. Interestingly, several new peaks of PANI appear in PANI-*g*-TCNF with varying TCNF content (2, 4, and 6 wt %) compared with TCNF. These are C═C stretching deformation of the quinoid ring at 1557, 1550, and 1555 cm^{-1}, C═C stretching deformation of the benzenoid ring at 1480, 1473, and 1473 cm^{-1}, and C−N stretching at 1293 cm^{-1} for PANI-*g*-TCNF with varying 2, 4, and 6 wt % of TCNF, respectively.[49] In addition, the band at 806 cm^{-1} and the low-intensity peaks in the range of 780−580 cm^{-1} can be ascribed to C−H out-of-plane bending vibrations and the C−H bond of the benzene ring, respectively. Interestingly, it is clearly noted that the benzenoid band is more intense than the quinoid band in a PANI-*g*-TCNF composite compared to neat PANI. Besides this, the peaks at around 1141, 1143, and 1140 cm^{-1} of different composites can be assigned to the N−Q−N−Q stretch of the quinoid ring, thereby confirming grafting of PANI on the surface of TCNF, as shown in Scheme 1, Step No-IV.[29] FTIR spectra of PANI−6XCNF and PANI-*g*-6TCNF composites were also collected for a comparison of van der Waals and covalent interactions. Interestingly, it is clearly observed from Figure 1d that there is no peak at around 1140 cm^{-1} corresponding to the N−Q−N−Q stretch of the quinoid ring, and the peak intensities of the benzenoid and quinoid bands in PANI−6XCNF are almost similar to that of PANI, thereby confirming the absence of covalent functionalization of PANI on the surface of XCNF for a PANI−6XCNF composite.[37]

In combination with FTIR spectroscopy, Raman scattering was measured to provide more information about the chemical bonding between TCNF and PANI. From Figure 2, it is clearly observed that significant structural changes occur during the chemical processing from CNF to XCNF, TCNF, and finally to PANI-*g*-TCNF composites with different weight percentages of TCNF. As expected, CNF displays two prominent peaks at 1351 and 1578 cm^{-1} corresponding to the well-defined D and G bands. The D band is related to the breathing mode of κ-point phonons of A_{1g} symmetry with vibrations of carbon atoms of dangling bonds in plane terminations of disordered and defected graphite.[50] The G mode corresponds to the allowed vibrations of a E_{2g} hexagonal graphite lattice. Importantly, it is observed that the intensity ratio of the D to G band (I_D/I_G) increases in XCNF, indicating the formation of more defects and greater disorder in XCNF, presumably because of excessive carboxylation. However, in the case of TCNF, there is an increase in I_G/I_D (1.030) compared with that of XCNF (0.845), suggesting an increase in the intimate interaction between TDI and XCNF.[51] The fewer defect also may be due to the removal of residuals from TCNFs during washing with anhydrous THF.[52] For PANI, the bands appear at 1595 and 1516 cm^{-1}, representing the C═C stretch of the quinoid and benzenoid rings, respectively.[53] The bands at 1390 and 1340 cm^{-1} are assigned to the $C-N^+$ stretching of polaronic forms of PANI.[53] However, in the Raman spectra of PANI-*g*-TCNF composites, the peaks corresponding to PANI are weak apart from the D and G bands and may be overlapped

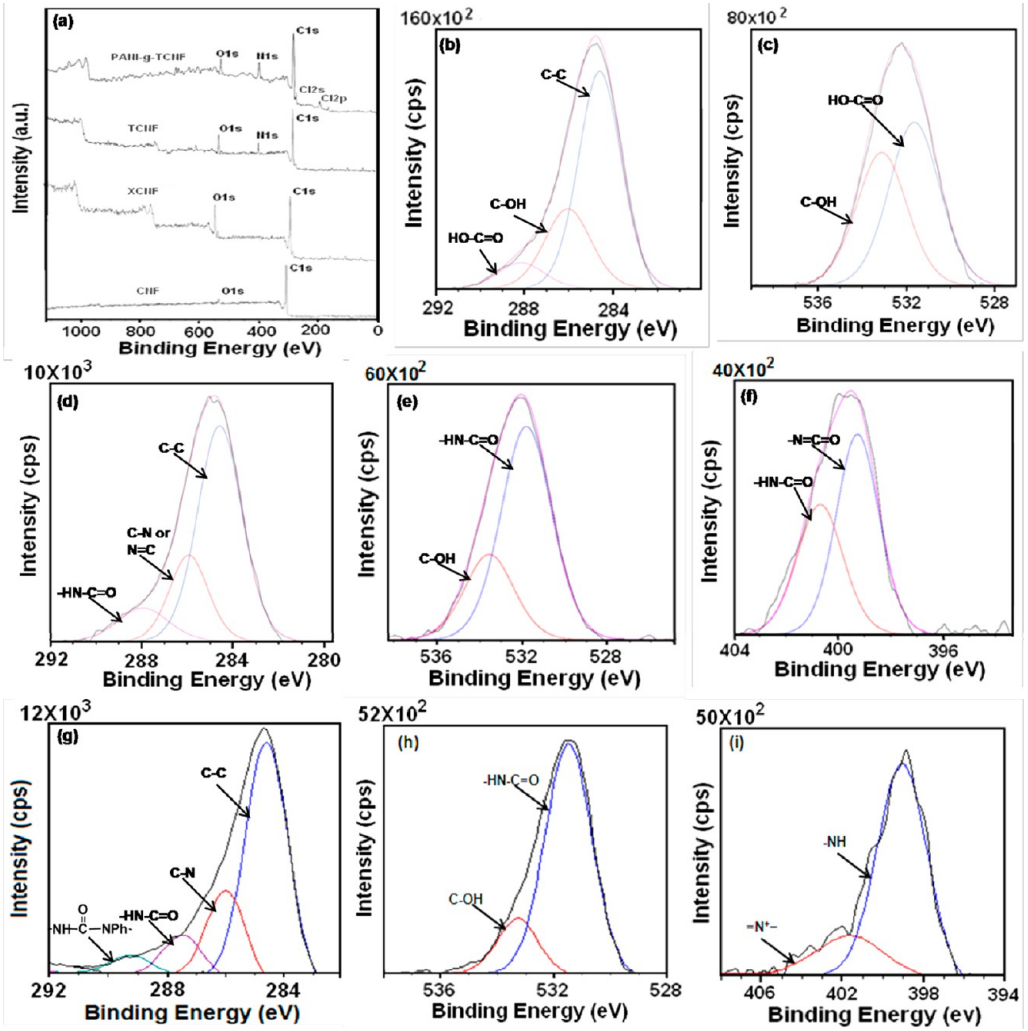

Figure 3. XPS spectra of (a) survey spectra of CNF, XCNF, TCNF, and PANI-*g*-TCNF and high resolute deconvoluted peaks for (b) C 1s and (c) O 1s of XCNF, (d) C 1s, (e) O 1s, and (f) N 1s of TCNF, and (g) C 1s, (h) O 1s, and (i) N 1s for a PANI-*g*-TCNF composite containing 6 wt % TCNF.

with TCNF peaks. However, I_D/I_G is almost unchanged in all of the composites with TCNF, suggesting the presence of fewer defects than XCNF carbon atoms, as noticed in a carboxyl-functionalized graphene oxide−PANI composite.[28] Interestingly, the D band of the composites shows blue shift from 1351 to 1369 cm^{-1} and the G band blue shifts from 1578 to 1589 cm^{-1}, suggesting electron transfer between PANI and TCNF because of the intimate interaction between them.[51] To achieve a clear representation, the spectra of CNF, XCNF, TCNF, and PANI-*g*-6TCNF were normalized in Figure 2B by taking the maximum value of the G band. On the contrary, there is no shifting of the D and G bands observed for a PANI−6XCNF composite compared to XCNF, confirming the absence of covalent interaction between XCNF and PANI (as shown in Figure S2 in the SI).

Figure S3 in the SI depicts the ^{1}H NMR spectra of PANI-*g*-TCNF composites containing 6 wt % TCNF in DMSO-d_6 in order to provide additional proof for the grafting of PANI on TCNF. The signals at 6.8, 7.0, and 7.3 ppm are assigned to the aromatic protons, which are due to the protons of PANI (both C−H and N−H) and TDI (C−H), as shown in Scheme 1, Step No-IV. Amide protons in different environments appear at 8.5 and 8.7 ppm, confirming the covalent functionaliztion of aniline with TDI.[47] Also, the aryl methyl proton signal appears at 1.2 ppm. All of these observations confirm the grafting of PANI on TCNF.

The XPS spectra of CNF, XCNF, TCNF, and a PANI-*g*-TCNF composite were obtained to verify the presence of the carboxyl group of XCNF, the amide group of TCNF and a PANI-*g*-TCNF composite, and PANI in the composite. Figure 3a shows XPS survey spectra for CNF, XCNF, TCNF, and a PANI-*g*-TCNF composite containing 6 wt % TCNF. It is found that the O/C atomic ratio decreases in the case of TCNF and further decreases in PANI-*g*-TCNF compared to XCNF, resulting in an increase of sp^2 carbon atoms on CNFs. This is further accompanied by the appearance of an N 1s peak at 400.0 eV for TCNF and PANI-*g*-TCNF. Interestingly, the N/C atomic ratio increases from TCNF to a PANI-*g*-TCNF composite, indicating the chemical bonding of PANI onto the TCNF surface. As a result, $\pi-\pi$ interaction is developed between TCNFs and PANI chains, facilitating charge transfer between them as well as providing the combined effect to the electrochemical behavior of the composites. These are in line with the earlier observations.[29,31] The high-resolution peak for C 1s and O 1s XPS spectra for CNF, XCNF, TCNF, and a PANI-*g*-TCNF composite and N 1s XPS spectra for TCNF and

dx.doi.org/10.1021/am4014049 | ACS Appl. Mater. Interfaces 2013, 5, 8374−8386

a PANI-*g*-TCNF composite are shown in Figure S4 in the SI and Figure 3b–i. In XCNF, the nonoxygeneted carbon centered at 284.6 e and −C−O at 286.0 eV, similar to that for CNF (as shown in Figure S4 in the SI). Interestingly, the peaks located at 288.2 and 531.8 eV corresponding to C 1s and O 1s of the −C═O (carboxyl) group in XCNF suggest successful carboxylation of CNF (as shown in Step No-I, Scheme 1). Notably, a peak located at 287.9 eV attributed to the −C═O bond of the amide group[54] and at 285.9 eV corresponding to C−N or N═C bond[55] for TCNF and the disappearance of the peak at 288.2 eV of the carboxyl group confirm functionalization of TDI with XCNF, as shown in Step No-II in Scheme 1. In addition, the deconvoluted peaks at 399.3 and 400.7 eV associated with the −N═C═O and −CONH bonds in the N 1s XPS spectra for TCNF suggest the presence of isocyanate and amide groups.[56] These findings further confirmed formation of the amide bond between the −NCO group of TDI and the −COOH group of XCNF. However, the ratio of [−N═C═O]:[−CONH] is slightly higher than 1 because of the presence of a trace amount of unreacted isocyanate in TCNF even after washing with anhydrous THF solvent to remove excess isocyanate. From the sensitivity factors for C 1s (0.25), O 1s (0.66), and N 1s (0.44), N/C and O/C of TCNF were calculated to be 15.12/56.26 and 28.60/54.26, respectively. Hence, half of the N/C atomic ratio (i.e., 7.56/54.26) participated in grafting with CNF. Therefore, the grafting level was calculated from XPS analysis based on the atomic percentage value for nitrogen and carbon atoms and was found to be 31.36%, which also agrees with the value obtained from FTIR analysis. In the case of survey spectra for PANI-*g*-TCNF composites (Figure 3a), chlorine is present along with carbon, nitrogen, and oxygen, indicating the presence of a doped state of PANI in the composite. Notably, the presence of peaks at 286.02 eV corresponding to the C−N bond of PANI, 287.55 eV for −CONH, and 289.2 eV for the urea moiety in the C 1s deconvoluted spectra for the composite (Figure 3g) confirms the covalent bonding of PANI with TCNF.[55,57] Additionally, the doped state of PANI in the composite is further inferred from the N 1s core level spectra at 401.6 eV related to protonated nitrogen (═N^+−). The lower amount of imine nitrogen atoms of a polyemeraldine base is preferentially protonated by HCl, which is indicated by the presence of a trace amount of chloride anions (197.2 eV) in the survey (Figure 3a) and deconvoluted Cl 2p spectra (Figure S5 in the SI) of the composite. These are also in line with the observations by Tan et al. and Kang et al.[58,59] The results from the XPS measurements reveal that the atomic percentage of ═N^+− is about 1.58, which is counterbalanced by the same amount of Cl^- anion present (1.54), leading to Cl^-/N^+ (0.975). The presence of protonated nitrogen in the composite is also consistent with the observations of An et al. and Tan et al.[51,59] The remaining nitrogen of the composite is due to the presence of the amine structure of PANI (17.54%), supporting the earlier observation.[51,58,59]

The interaction between PANI and TCNF is further proved by taking UV−visible spectra of PANI and PANI-*g*-TCNF (6 wt %) at different times (1 min, 5 min, 15 min, 30 min, 1 h, 2 h, 3 h, 12 h, and 24 h) during polymerization (as shown in Figure S6 in the SI). PANI presents two absorption bands at 305 and 410 nm corresponding to the benzenoid−quinoid $\pi-\pi^*$ transition and a low-wavelength polaron band,[60] respectively, and the intensities of the bands decrease with time. On the contrary, the absorption bands corresponding to PANI are red-shifted to 312 and 420 nm in a PANI-*g*-TCNF composite similar to earlier reported PANI−graphene composites,[61] and the intensities of those bands decrease with time. Besides this, the intensity of the peak is also lowered compared to that of PANI, suggesting covalent interaction between PANI and TCNF.

XRD patterns of pristine CNF, XCNF, and TCNF are presented in Figure 4. Pristine CNF shows an intense and sharp

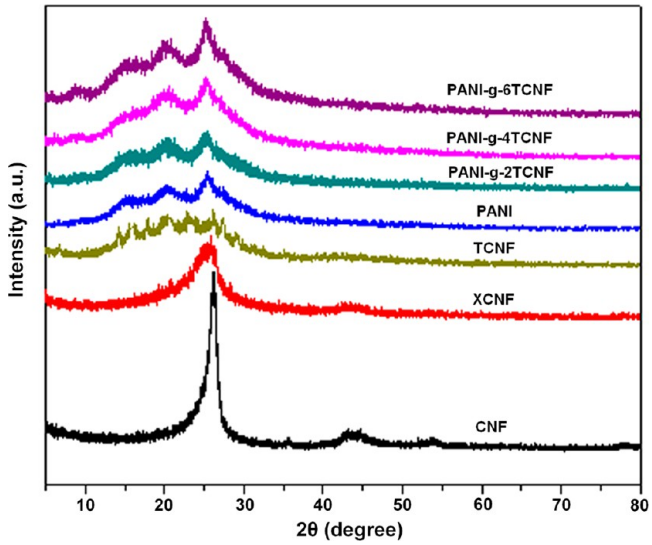

Figure 4. XRD patterns of CNF, XCNF, TCNF, PANI, and composites containing 2, 4, and 6 wt % TCNF.

peak at 26.2° and two characteristic peaks at 43.8° and 53.8° corresponding to (002), (101), and (004) planes of hexagonal graphite, respectively.[62] A similar XRD pattern is observed in the case of XCNF; only a slight shifting of 2θ around 25.7° with broadening was observed, suggesting that a significant portion of CNF is carboxylated. However, in the case of TCNF, the peak is relatively more broadened than the earlier one with increased amorphousness, indicating successful modification of XCNF by TDI. Amorphous PANI exhibits broad intense peaks at 2θ = 15°, 20.3°, and 25.4° related to (011), (020), and (200) planes, which are also the characteristic Bragg diffraction peaks of the reported PANI.[29] Similar findings are also noted for PANI-*g*-TCNF composites containing 2, 4, and 6 wt % TCNF, indicating the successful reaction of PANI on TCNF. Interestingly, with increasing content of TCNF, the peak intensity corresponding to PANI increases. This may be due to the increased grafting ability of PANI on TCNF with increasing content of TCNF.

To visually investigate the dimensional self-construction of the as-received CNF, resulting XCNF, TCNF, and PANI, and finally the as-synthesized PANI-*g*-6TCNF composite, the surface morphology of each sample was imaged, as shown in Figure 5 for comparison. It is observed that CNF has a fibrillar structure with a diameter in the range of 110 ± 40 nm and a length of several micrometers. In the case of XCNF, the morphology does not appear to be altered from CNF by mixed acid treatment like previous findings.[43,44] However, after functionalization with TDI (TCNF), a significant change of the morphology is observed and the surface of the fiber becomes rough, indicating modification by organic moieties. The diameter of the functionalized fibers increases by about

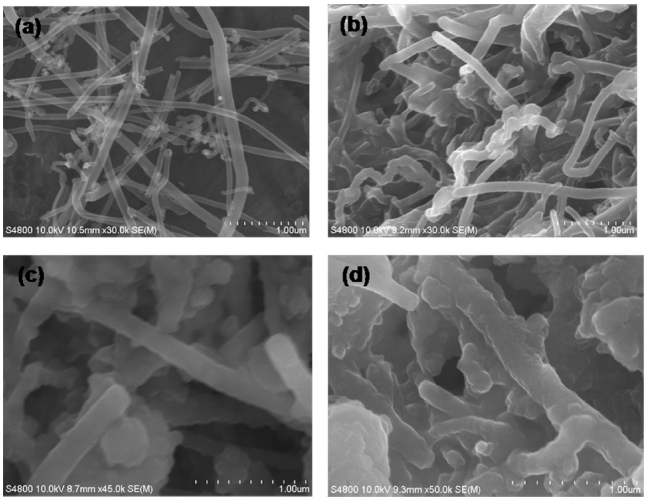

Figure 5. FESEM images of (a) CNF, (b) XCNF, (c) TCNF, and (d) a PANI-*g*-TCNF composite containing 6 wt % TCNF.

40−90 nm. This observation also supports earlier literature on organic functionalized CNTs.[63] For the PANI-*g*-6TCNF composite, the microstructure is markedly affected by the chemical bonding of PANI with TCNF. This is because of the fact that the hydrophobic CNF is changed to hydrophilic CNF by carboxylation and made more hydrophilic by functionalization with TDI. As a result, there is a strong interaction between hydrophilic TCNF and hydrophilic PANI. The FESEM image (as shown in Figure 5d) reveals that PANI is well distributed on the TCNF surface with variation in the diameter of 170 ± 60 nm. The distribution of PANI on TCNF is also uniform in PANI-*g*-2TCNF and PANI-*g*-4TCNF composites (as shown in Figure S7 in the SI). The grafting of PANI on TCNF facilitates stronger interaction between the two components, which leads to uniform distribution of PANI on TCNF by growing PANI chains on the TCNF surface. In addition, such an interaction is very efficient to decrease the charge-transfer barrier and thereby accelerate charge transfer and is expected to improve the electrochemical cycling stability of the composites.[64]

The interaction between TCNF and PANI was further realized by analyzing the microstructure of bare TCNF along with a PANI-*g*-TCNF composite containing 6 wt % TCNF using tapping-mode AFM. From their phase morphology shown in Figure 6, it is clearly observed that TCNF is aligned in such a way that most of the nanofibers are contacted at the tip rather than the side wall. The diameter of TCNF is in the range of 190 ± 50 nm. However, the composite exhibits an intimate contact between PANI and TCNF, providing variation in the diameter of about 180 ± 45 nm. This observation also reveals strong interaction between these hydrophilic components through chemical bonding, well supporting the earlier study.[65] Therefore, PANI is uniformly distributed onto the entire TCNF surface, leading to an increase in the rate of charge transfer.

Further, TEM was used for more clear identification of the morphology of the as-synthesized materials. TEM images of CNF and XCNF (as shown in Figure S8 in the SI) exhibit fibrillar structure, although XCNF represents some corrugated morphology because of distraction of the sp^2 carbon atoms by carboxylation, in line with earlier literature.[29,36] However, after functionalization with TDI, the morphology is significantly changed because of the introduction of TDI on the XCNF surface, as is evident from Figure 7a. Conversely, after grafting

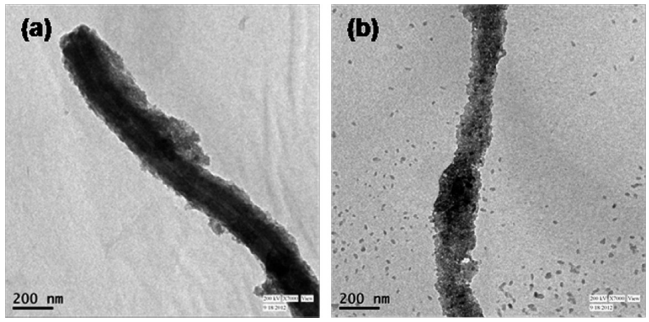

Figure 7. TEM images of (a) TCNF and (b) a PANI-*g*-TCNF composite containing 6 wt % TCNF.

with PANI on TCNF as shown in Figure 7b, a remarkable change in the morphology reveals the introduction of PANI on TCNF surfaces. It is clearly visible that PANI is uniformly distributed on the surface of the TCNF host. The intimate contact between TCNF and PANI provides relatively short path lengths for electronic transport to improve utilization of the electrodes as capacitors.

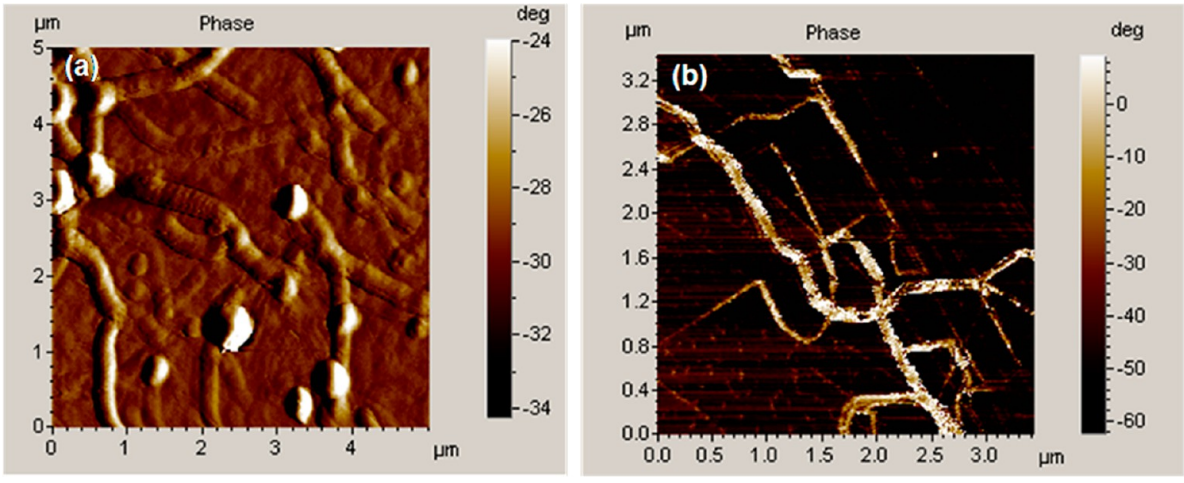

Figure 6. AFM images of (a) TCNF and (b) a PANI-*g*-TCNF composite containing 6 wt % TCNF.

dx.doi.org/10.1021/am4014049 | ACS Appl. Mater. Interfaces 2013, 5, 8374−8386

Mass loss under a N_2 atmosphere and the grafting of PANI on TCNF were determined thermogravimetrically. As shown in Figure 8, pristine CNF exhibits maximum thermal stability

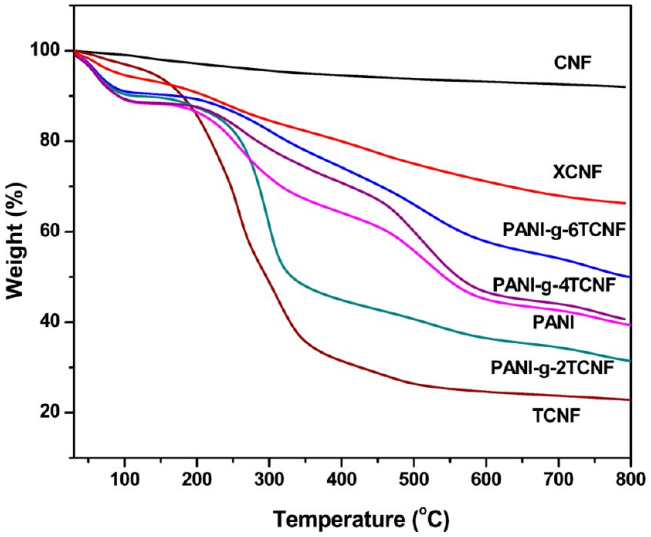

Figure 8. TGA plots of CNF, XCNF, TCNF, PANI, and PANI-*g*-TCNF composites containing 2, 4, and 6 wt % TCNF at a heating rate of 10 °C min^{-1} under a N_2 atmosphere.

because there is no decomposition in the temperature range of 50−800 °C. Except CNF and TCNF, all of the materials show a little mass loss around 100 °C due to the evaporation of surface-absorbed water molecules. In the case of XCNF, it shows almost 30% mass loss compared to CNF (9%) due to the decomposition of carboxyl groups in the temperature range of 50−800 °C. At the same time, TCNF shows dramatic (77%) mass loss for the decomposition of carboxyl and isocyanate groups.[66] For PANI, a mass loss of 58% is observed from 50 to 800 °C. However, it shows gradual weight loss between 100 and 225 °C owing to the deprotonation of PANI losing dopant HCl and major weight loss of about 35% prior to 600 °C assigned to the decomposition of PANI with various polymerization degrees,[67] although at the same time PANI-*g*-TCNF composites containing 2, 4, and 6 wt % TCNF show relatively lower weight loss between 100 and 225 °C corresponding to the deprotonation of PANI, confirming the grafting of PANI on TCNF. In addition, these composites present 68.5, 57, and 52% mass loss, i.e., relatively slower mass loss compared to TCNF in the temperature range of 50−800 °C due to the decomposition of TCNF components in the composites. Therefore, PANI-*g*-TCNF containing 6 wt % TCNF shows the best thermal stability among all of the composites because of more grafting of PANI on TCNFs.

The electrochemical performances of the as-prepared PANI-*g*-TCNF composites along with PANI, TCNF, and CNF were analyzed using CV, GCD, and EIS measurements. From the CV curves shown in Figure 9a, an amazing difference in the electrochemical surface activity among the composites, PANI, TCNF, and CNF can easily be identified. It is noted that the areas of the CV curves of PANI-*g*-TCNF composites are larger than that of individual PANI, TCNF, or CNF, indicating a better capacitive response for PANI-*g*-TCNF composites, demonstrating significant synergistic effect of PANI and TCNF. However, it is found that PANI-*g*-TCNF having 6 wt % TCNF exhibits the largest capacity among all of the composites without altering the shape of the CV profiles. Notably, PANI−6XCNF exhibits a much lower area of the CV curve than that of PANI-*g*-6TCNF, indicating the better capacitance performance of the PANI-*g*-6TCNF composite, and thereby the functionalization of XCNF with TDI is useful in enhancing the capacitance performance of the composite. The intimate interaction or strong charge coupling of PANI with TCNF arising from the chemical bonding provides a synergistic effect and results in enhanced accessibility of the electrolyte by every PANI nanoparticle, leading to improved capacitance of the composites.[51] On the contrary, the poor interaction between PANI and XCNF results in a lower CV current and thereby an inferior specific capacitance. In the case of CNF and TCNF, only one pair of weak redox peaks arises, suggesting the transition between quinone and hydroquinone groups.[14] In contrast, the CV curves of PANI, PANI−6XCNF, and PANI-*g*-TCNF composites present two couples of well-defined redox peaks due to the redox transformation of the

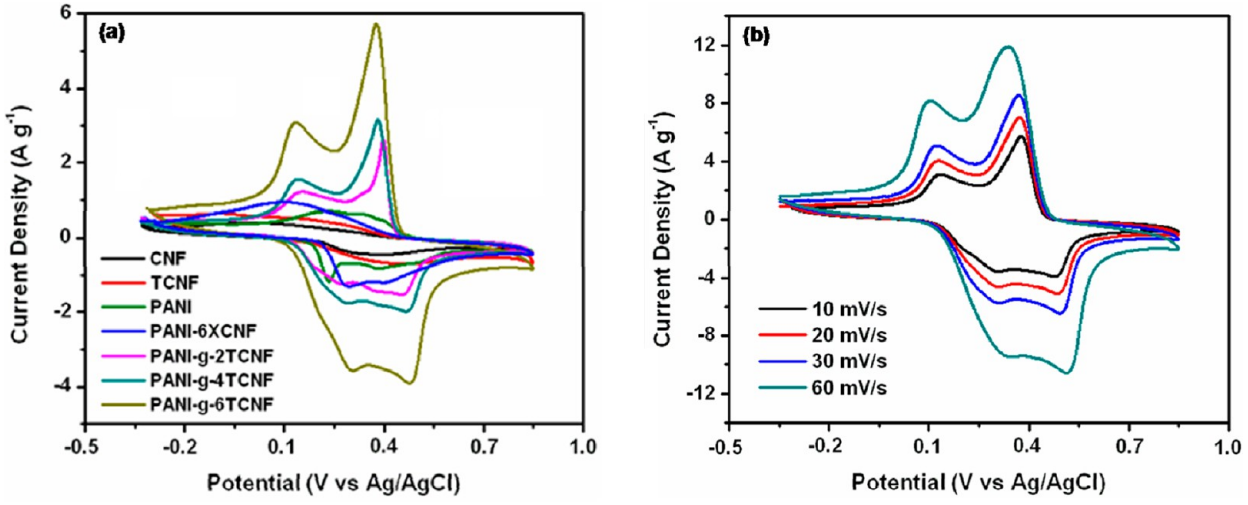

Figure 9. Cyclic voltammograms recorded in a 1 M H_2SO_4 solution as the electrolyte (a) at a sweep rate of 10 mV s^{-1} of CNF, TCNF, PANI, PANI−6XCNF, and PANI-*g*-TCNF composites having 2, 4, and 6 wt % TCNF and (b) at different scan rates for a PANI-*g*-TCNF composite having 6 wt % TCNF.

dx.doi.org/10.1021/am4014049 | ACS Appl. Mater. Interfaces 2013, 5, 8374−8386

leucoemeraldine/emeraldine and emeraldine/pernigraniline forms, respectively. Such an electrochemical response gives rise to a pseudocapacitive effect in PANI.[14,26]

Moreover, the CV plots of the PANI-*g*-TCNF composite containing 6 wt % TCNF at different scan rates were also analyzed, as displayed in Figure 9b. The general features of the composite voltammogram remain unchanged even at high scan rates. Interestingly, a remarkable difference of the electrochemical surface activity has been noted in terms of very high capacitance and stable performance in our prepared PANI-*g*-TCNF composite than in earlier reported PANI-*g*-CNT[68] and PANI-*g*-reduced graphite oxide[29] composites. Such good rate capability for the composite indicates the stability of the conjugated structure formed by chemical bonding, leading to enhanced electronic transport even at high scan rate.[64]

The EIS response was analyzed in terms of Nyquist plots showing the frequency response characteristics at the electrode−electrolyte interface and is provided in Figure 10.

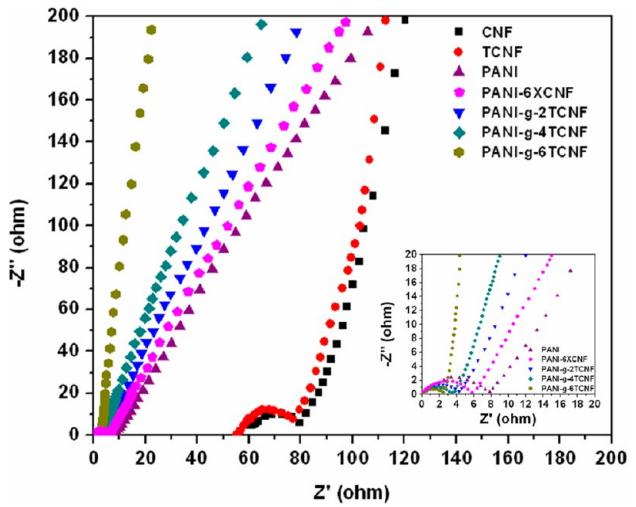

Figure 10. Nyquist plots recorded from 10^5 to 0.001 Hz with an ac amplitude of 5 mV for CNF, TCNF, PANI, PANI−6XCNF, and PANI-*g*-TCNF composites containing 2, 4, and 6 wt % TCNF.

It is observed that the Nyquist plots of TCNF, PANI, PANI−6XCNF, and PANI-*g*-TCNF composites show a semicircular arc at high frequency followed by almost a linear spike at higher frequency. A steep vertical line along the imaginary axis corresponds to the ideal capacitor. The 45°-sloped portion of the Nyquist plots, known as the Warburg resistance, is larger in the case of CNF, TCNF, PANI, and PANI−6XCNF than PANI-*g*-TCNF composites (as shown in Figure 10 and its inset), suggesting greater variation in the ion diffusion path lengths and increased obstruction to the ionic movement in PANI−6XCNF, PANI, TCNF, and CNF. Interestingly, the semicircular arc at high frequency is not detected in a PANI-*g*-TCNF composite containing 6 wt % TCNF, suggesting that the interfacial charge-transfer resistance in that composite is significantly low because of the prevention of charge accumulating through the chemical bonding between PANI and TCNF.[51] This observation is corroborated by morphology analysis (already discussed earlier) where PANI is distributed homogeneously on TCNF. In addition, the presence of a high content of TCNF in PANI, leading to a larger amount of distributed PANI, is also responsible for the minimal charge-transfer barrier of the composite. On the contrary, the higher charge-transfer resistance of PANI−6XCNF compared to that of the PANI-*g*-6TCNF composite implies that poor interaction causes insufficient linkup between PANI and XCNF for charge migration.[28] Meanwhile, the equivalent series resistance of CNF is larger because of lesser diffusibility of the electrolyte into the CNF network compared to the PANI-*g*-TCNF network, highlighting the efficiency of grafting of PANI on the TCNF surface.

Figure 11a shows the GCD plots at a current density of 0.3 A g^{-1}. It is observed that the specific capacitance of a PANI-*g*-TCNF composite using eq 1 is superior to those of PANI−6XCNF, PANI, CNF, and TCNF. Noticeably, the discharge curve of composites exhibits two clear voltage stages: a fast potential drop and a slow potential decay. The first one with relatively short discharge duration is assigned to the EDL capacitance of the electrode, while the latter one with a much longer discharging duration is ascribed to the combination of EDL and Faradic capacitances of the PANI component.[69] Interestingly, the "IR drop" is higher in PANI than in a PANI-*g*-

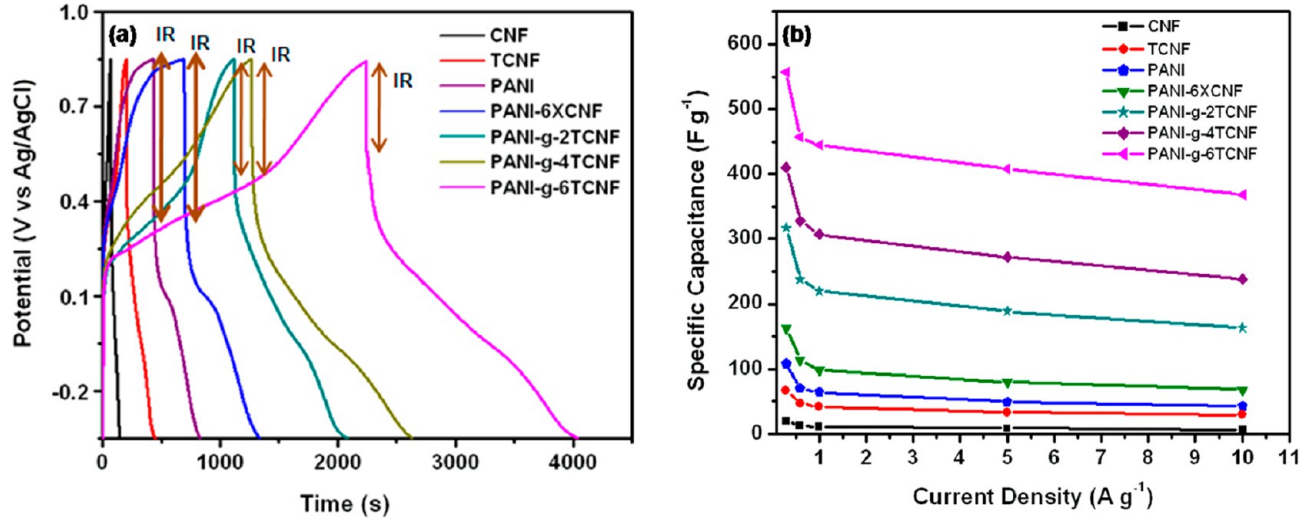

Figure 11. (a) GCD plots at a current density of 0.3 A g^{-1} and (b) variation of the specific capacitance with the current density of CNF, TCNF, PANI, PANI−6XCNF, and PANI-*g*-TCNF composites having 2, 4, and 6 wt % TCNF.

dx.doi.org/10.1021/am4014049 | ACS Appl. Mater. Interfaces 2013, 5, 8374−8386

TCNF composite, indicating the effectiveness of the synergistic combination of TCNF and PANI through chemical bonding. At 0.3 A g^{-1} current density, a PANI-*g*-6TCNF composite exhibits the highest specific capacitance (557 F g^{-1}), almost 5.16 times higher than that of PANI and 8.29 times higher than that of TCNF, indicating a significant synergistic effect. Interestingly, the specific capacitance of the as-prepared composites is superior to that of graphene−PANI composites (480 F g^{-1} at 0.1 A g^{-1}) formed by van der Waals force[17] and graphene−polypyrrole−carbon nanotube (GN−PPy−CNT) ternary composites (361 F g^{-1} at 0.2 A g^{-1}).[70] Such a high specific capacitance is probably due to the synergistic effect of PANI and TCNF and the grafting of PANI on TCNFs via a phenyl-substituted amide linkage. On the contrary, the 3.44 times higher specific capacitance of a PANI-*g*-6TCNF composite than that of PANI−6XCNF further confirms that the chemical bonding in the former case promotes the capacitance performance.[64] The rate performance of the samples is further evaluated by charging−discharging at different current densities, as revealed in Figure 11b. It is clearly observed that in all cases the specific capacitance decreases with an increase in the discharge current density. At the highest current density of 10 A g^{-1}, the capacitance retention is still 51%, 58%, and 66% for PANI-*g*-TCNF composites having 2, 4, and 6 wt % TCNF, while the retention is still 42% for PANI−6XCNF. The high rate capability of a PANI-*g*-6TCNF composite prepared using a covalent technique compared to that of PANI−6XCNF interconnected by van der Waals attraction indicates the superiority of the materials by making intimate interaction through formation of the π-conjugated system between PANI and TCNF. Thus, it can be inferred that a supercapacitor designed on the electrode in the present work has a better rating in terms of rapid ion diffusion, faster charge−discharge kinetics, and very large capacitance.

The capacitor response and its better rating have further been confirmed in terms of its cycling performance. The cycling capacitance performance of the as-prepared PANI-*g*-TCNF composites with different loadings of TCNF along with PANI and TCNF has been studied with up to 2000 charge−discharge cycles at a current density of 0.3 A g^{-1}. From Figure 12, it is observed that, after 2000 charge−discharge cycles, PANI, PANI−6XCNF, and PANI-*g*-TCNF containing 2, 4, and 6 wt % TCNF retain 17% (18 F g^{-1}), 56% (91 F g^{-1}), 74% (235 F g^{-1}), 81% (332 F g^{-1}), and 86% (479 F g^{-1}) of their initial capacitance, respectively. These results demonstrate that the chemical anchoring effect as well as the synergistic effect of PANI and TCNF promotes the electrochemical stability of the PANI-*g*-TCNF composites over PANI−6XCNF. Interestingly, the specific capacitance of a PANI-g-TCNF composite containing 6 wt % TCNF is the highest among all of the composites, suggesting the advantages of a synergistic combination of the EDL capacitance of TCNF and pseudocapacitance of PANI through grafting of PANI on TCNF.

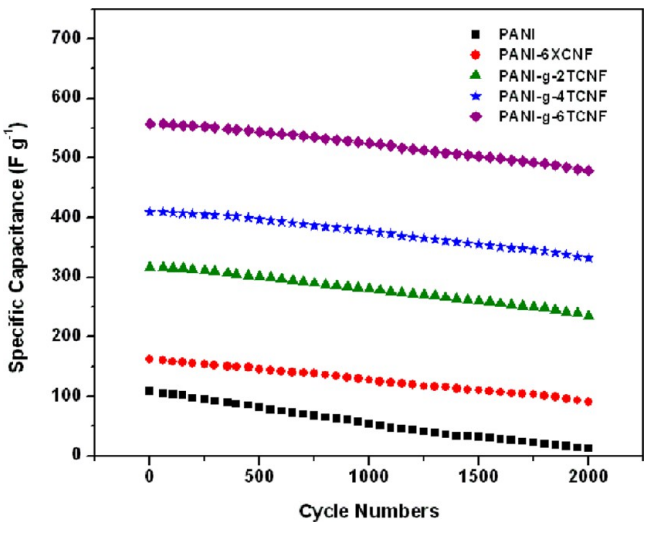

Figure 12. Capacitance-retaining performance with charge−discharge cycling at a current density of 0.3 A g^{-1}.

CONCLUSIONS

A novel and facile synthetic route was established for the synthesis of highly efficient supercapacitor PANI-*g*-TCNF composites. Such promising composites were prepared by functionalizing XCNF with TDI through amidation followed by reaction with excess aniline to form a urea derivative and residual aniline, which was subsequently polymerized and grafted with a urea derivative. The strategy on amidation of CNF and, consequently, the grafting of PANI on TCNF were verified by FTIR, Raman, ^{1}H NMR, XPS, and XRD. Also, the sound interaction between TCNF and PANI, leading to the uniform distribution of PANI on the TCNF surface, was further confirmed by FESEM, AFM, and TEM, resulting in fast charge transfer and rapid ion diffusion. TGA showed higher thermal stability of the composite compared to those of PANI and CNF. A maximum capacitance of 557 F g^{-1} and good cycling stability (retention of 86% of its initial capacitance event after 2000 cycles) are observed for a PANI-*g*-TCNF composite containing 6 wt % TCNF due to the strong interaction between TCNF and PANI by chemical grafting as well as their synergistic contribution. Their supercapacitor performance was found to be superior to the materials formed by van der Waals forces. The present study also encourages their applications in optoelectronic devices and in sensors.

ASSOCIATED CONTENT

Supporting Information

Calibration curve for determining the grafting percentage of TDI on XCNF, Raman spectra of XCNF, PANI, and PANI−6XCNF,^{1}H NMR spectra of a PANI-*g*-6TCNF composite, XPS of high resolute deconvoluted peaks for (a) C 1s and (b) O 1s for CNF, XPS of the high resolute deconvoluted peak for Cl 2p of the composite, UV−visible spectra of PANI and PANI-*g*-TCNF (6 wt %) at different times (1 min, 5 min, 15 min, 30 min, 1 h, 2 h, 3 h, 12 h, and 24 h) during polymerization, FESEM images of PANI-*g*-2TCNF and PANI-*g*-4TCNF composites, and TEM images of CNF and XCNF. This material is available free of charge via the Internet at http://pubs.acs.org.

AUTHOR INFORMATION

Corresponding Author

*E-mail: director@iitp.ac.in. Tel.: (+91-6122) 277380. Fax: (+91-6122) 277384.

Notes

The authors declare no competing financial interest.

■ ACKNOWLEDGMENTS

The authors gratefully acknowledge IIT Patna, India, and an Indo−Australia grant for financial support. The authors thank the Central Research Facility, IIT Kharagpur, India, for carrying out TEM analysis.

■ REFERENCES

(1) Simon, P.; Gogotsi, Y. *Nat. Mater.* **2008**, *7*, 845−854.
(2) Zhang, L. L.; Zhao, X. S. *Chem. Soc. Rev.* **2009**, *38*, 2520−2531.
(3) Zheng, F. L.; Li, G. R.; Ou, Y. N.; Wang, Z. L.; Su, C. Y.; Tong, Y. X. *Chem. Commun.* **2010**, *46*, 5021−5023.
(4) Liu, R.; Duay, J.; Lee, S. B. *Chem. Commun.* **2011**, *47*, 1384−1404.
(5) Pandolfo, A. G.; Hollenkamp, A. F. *J. Power Sources* **2006**, *157*, 11−27.
(6) Dunn, B.; Kamath, H.; Tarascon, J. M. *Science* **2011**, *334*, 928−935.
(7) Frackowiak, E. *Phys. Chem. Chem. Phys.* **2007**, *9*, 1774−1785.
(8) Conway, B. E. *Electrochemical Supercapacitors: Scientific Fundamentals and Technological Applications*; Kluwer-Plenum: New York, 1999.
(9) Beck, F.; Rüetschi, P. *Electrochim. Acta* **2002**, *45*, 2467−2482.
(10) Yang, C. M.; Kim, Y. J.; Endo, M.; Kanoh, H.; Yudasaka, M.; Iijima, S.; Kaneko, K. *J. Am. Chem. Soc.* **2007**, *129*, 20−21.
(11) Gao, H.; Xiao, F.; Ching, C. B.; Duan, H. *ACS Appl. Mater. Interfaces* **2012**, *4*, 7020−7026.
(12) Lee, J. W.; Hall, A. S.; Kim, J. D.; Mallouk, T. E. *Chem. Mater.* **2012**, *24*, 1158−1164.
(13) Lee, M. T.; Fan, C. Y.; Wang, Y. C.; Li, H. Y.; Chang, J. K.; Tseng, C. M. *J. Mater. Chem. A* **2013**, *1*, 3395−3405.
(14) Wang, D. W.; Li, F.; Zhao, J. P.; Ren, W. C.; Chen, Z. G.; Tan, J.; Wu, Z. S.; Gentle, I.; Lu, G. Q.; Cheng, H. M. *ACS Nano* **2009**, *3*, 1745−1752.
(15) Ertas, M.; Walczak, R. M.; Das, R. K.; Rinzler, A. G.; Reynolds, J. R. *Chem. Mater.* **2012**, *24*, 433−443.
(16) Frackowiak, E.; Khomenko, V.; Jurewicz, K.; Lota, K.; Beguin, F. *J. Power Sources* **2006**, *153*, 413−418.
(17) Zhang, K.; Zhang, L. L.; Zhao, X. S.; Wu, J. *Chem. Mater.* **2010**, *22*, 1392−1401.
(18) Snook, G. A.; Kao, P.; Best, A. S. *J. Power Sources* **2011**, *196*, 1−12.
(19) Fan, W.; Zhang, C.; Tjiu, W. W.; Pramoda, K. P.; He, C.; Liu, T. *ACS Appl. Mater. Interfaces* **2013**, *5*, 3382−3391.
(20) Xu, J. J.; Wang, K.; Zu, S. Z.; Han, B. H.; Wei, Z. X. *ACS Nano* **2010**, *4*, 5019−5026.
(21) Yan, X.; Chen, J.; Yang, J.; Xue, Q.; Miele, P. *ACS Appl. Mater. Interfaces* **2010**, *2*, 2521−2529.
(22) Zhu, J.; Gu, H.; Luo, Z.; Haldolaarachige, N.; Young, D. P.; Wei, S.; Guo, Z. *Langmuir* **2012**, *28*, 10246−10255.
(23) Yan, Y.; Cheng, Q.; Wang, G.; Li, C. *J. Power Sources* **2011**, *196*, 7835−7840.
(24) Romero, P. G.; Ayyad, O.; Guevara, J. S.; Muñoz, R. D. *J. Solid State Electrochem.* **2010**, *14*, 1939−1945.
(25) Nyholm, L.; Nystrom, G.; Mihranyan, A.; Strømme, M. *Adv. Mater.* **2011**, *23*, 3751−3769.
(26) Wang, Y. G.; Li, H. Q.; Xia, Y. Y. *Adv. Mater.* **2006**, *18*, 2619−2623.
(27) Li, Z. F.; Zhang, H.; Liu, Q.; Sun, L.; Stanciu, L.; Xie, J. *ACS Appl. Mater. Interfaces* **2013**, *5*, 2685−2691.
(28) Liu, Y.; Deng, R.; Wang, Z.; Liu, H. *J. Mater. Chem.* **2012**, *22*, 13619−13624.
(29) Kumar, N. A.; Choi, H. J.; Shin, Y. R.; Chang, D. W.; Dai, L.; Baek, J. B. *ACS Nano* **2012**, *6*, 1715−1723.
(30) Li, L.; Qin, Z. Y.; Liang, X.; Fan, Q. Q.; Lu, Y. Q.; Wu, W. H.; Zhu, M. F. *J. Phys. Chem. C* **2009**, *113*, 5502−5507.
(31) Wang, H.; Hao, Q.; Yang, X.; Lu, L.; Wang, X. *Nanoscale* **2010**, *2*, 2164−2170.
(32) Cheng, Q.; Tang, J.; Ma, J.; Zhang, H.; Shinya, N.; Qin, L. C. *J. Phys. Chem. C* **2011**, *115*, 23584−23590.
(33) Sengupta, R.; Bhattacharya, M.; Bhowmick, A. K. *Prog. Polym. Sci.* **2011**, *36*, 638−670.
(34) Roy, N.; Sengupta, R.; Bhowmick, A. K. *Prog. Polym. Sci.* **2012**, *37*, 781−819.
(35) Choi, Y. K.; Sugimoto, K.; Song, S. M.; Ohkoshi, Y.; Endo, M. *Carbon* **2005**, *43*, 2199−2208.
(36) Jang, J.; Bae, J.; Choi, M.; Yoon, S. H. *Carbon* **2005**, *43*, 2730−2736.
(37) Du, X.; Liu, H. Y.; Cai, G.; Mai, Y. W.; Baji, A. *Nanoscale Res. Lett.* **2012**, *7*, 111−118.
(38) Wu, Q.; Xu, Y. X.; Yao, Z. Y.; Liu, A. R.; Shi, G. Q. *ACS Nano* **2010**, *4*, 1963−1970.
(39) Gupta, V.; Miura, N. *Electrochim. Acta* **2006**, *52*, 1721−1726.
(40) Biswas, S.; Drazal, L. T. *Chem. Mater.* **2010**, *22*, 5667−5671.
(41) Otero, T. F.; Padilla, J. *J. Electroanal. Chem.* **2004**, *561*, 167−171.
(42) Liu, J.; Rinzler, A. G.; Dai, H.; Hafner, J. H.; Bradley, R. K.; Boul, P. J.; Lu, A.; Iverson, T.; Shelimov, K.; Huffman, C. B.; Rodriguez-Macias, F.; Shon, Y. S.; Lee, T. R.; Colbert, D. T.; Smalley, R. E. *Science* **1998**, *280*, 1253−1256.
(43) Rasheed, A.; Howe, J. Y.; Dadmun, M. D.; Britt, P. F. *Carbon* **2007**, *45*, 1072−1080.
(44) Guha, A.; Lu, W.; Zawodzinski, T. A.; Schiraldi, D. A. *Carbon* **2007**, *45*, 1506−1517.
(45) Matsuo, Y.; Miyabe, T.; Fukutsuka, T.; Sugie, Y. *Carbon* **2007**, *45*, 1005−1012.
(46) Boccara, A. C.; Fournier, D.; Kumar, A.; Pandey, G. C. *J. Appl. Polym. Sci.* **1998**, *63*, 1785−1791.
(47) Kotal, M.; Srivastava, S. K. *J. Mater. Chem.* **2011**, *21*, 18540−18551.
(48) Kim, A.; Filler, M. A.; Kim, S.; Bent, S. F. *J. Am. Chem. Soc.* **2005**, *127*, 6123−6132.
(49) Wang, D. Y.; Caruso, F. *Adv. Mater.* **2001**, *13*, 350−354.
(50) Tuinstra, F. *J. Chem. Phys.* **1970**, *53*, 1126−1130.
(51) An, J.; Liu, J.; Zhou, Y.; Zhao, H.; Ma, Y.; Li, M.; Yu, M.; Li, S. *J. Phys. Chem. C* **2012**, *116*, 19699−19708.
(52) Canto, E. D.; Flavin, K.; Movia, D.; Navio, C.; Bittencourt, C.; Giordani, S. *Chem. Mater.* **2011**, *23*, 67−74.
(53) Cochet, M.; Louarn, G.; Quillard, S.; Buisson, J. P.; Lefrant, S. *J. Raman Spectrosc.* **2000**, *31*, 1041−1049.
(54) Baker, E. S.; Cai, W.; Lasseter, T. L.; Weidkamp, K. P.; Hamers, R. J. *Nano Lett.* **2002**, *2*, 1413−1417.
(55) Zhou, X.; Wu, T.; Hu, B.; Yang, G.; Han, B. *Chem. Commun.* **2010**, *46*, 3663−3665.
(56) Ikeo, N.; Iijima, Y.; Niimura, N.; Shigematsu, M.; Tazawa, T.; Matsumoto, S.; Kojima, K.; Nagasawa, Y. *Handbook of X-ray Photoelectron Spectroscopy*; JEOL: Tokyo, 1991.
(57) Wen, J.; Somorjai, G.; Lim, F.; Ward, R. *Macromolecules* **1997**, *30*, 7206−7213.
(58) Kang, E. T.; Neoh, K. G.; Tan, K. L. *Surf. Interface Anal.* **1992**, *19*, 33−37.
(59) Tan, K. L.; Tan, B. T. G.; Kang, E. T.; Neoh, K. G. *Phys. Rev. B* **1989**, *39*, 8070−8073.
(60) Stafstrom, S.; Bredas, J. L.; Epstein, A. J.; Woo, H. S.; Tanner, D. B.; Huang, W. S.; MacDiarmid, A. G. *Phys. Rev. Lett.* **1987**, *59*, 1464−1467.
(61) Zhou, X.; Wu, T.; Hu, B.; Yang, G.; Han, B. *Chem. Commun.* **2010**, *46*, 3663−3665.
(62) Rajarao, R.; Bhat, B. R. *Nanomater. Nanotechnol.* **2012**, *2*, 1−6.
(63) Georgakilas, V.; Kordatos, K.; Prato, M.; Guldi, D. M.; Holzinger, M.; Hirsch, A. *J. Am. Chem. Soc.* **2002**, *124*, 760−761.
(64) Jianhua, L.; Junwei, A.; Yecheng, Z.; Yuxiao, M.; Mengliu, L.; Mei, Y.; Songmei, L. *ACS Appl. Mater. Interfaces* **2012**, *4*, 2870−2876.
(65) Yun, J.; Im, J. S.; Kim, H. I.; Lee, Y. S. *Appl. Surf. Sci.* **2012**, *258*, 3462−3468.
(66) Che, J.; Yuan, W.; Jiang, G.; Dai, J.; Lim, S. Y.; Chan-Park, M. B. *Chem. Mater.* **2009**, *21*, 1471−1479.

(67) Yang, C. Y.; Reghu, M.; Hegger, A. J.; Cao, Y. *Synth. Met.* **1996**, *79*, 27−32.
(68) Xiong, S.; Wei, J.; Jia, P.; Yang, L.; Ma, J.; Lu, X. *ACS Appl. Mater. Interfaces* **2011**, *3*, 782−788.
(69) Gao, Z.; Yang, W.; Wang, J.; Wang, B.; Li, Z.; Liu, Q.; Zhang, M.; Liu, L. *Energy Fuels* **2013**, *27*, 568−575.
(70) Lu, X.; Zhang, F.; Dou, H.; Yuan, C.; Yang, S.; Hao, L.; Shen, L.; Zhang, L.; Zhang, X. *Electrochim. Acta* **2012**, *69*, 160−166.